ISCI, Volume *11*

Supplemental Information

Srv2 Is a Pro-fission Factor that Modulates Yeast Mitochondrial Morphology and Respiration by Regulating Actin Assembly

Ying-Chieh Chen, Tzu-Hao Cheng, Wei-Ling Lin, Chang-Lin Chen, Wei Yuan Yang, Craig Blackstone, and Chuang-Rung Chang

Supplemental Figure 1.

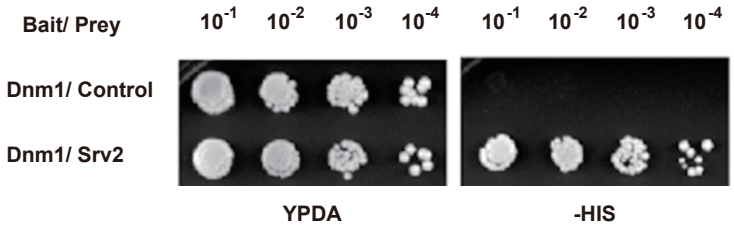

Figure S1. Yeast two-hybrid analysis to identify Srv2-Dnm1 interaction, related to Figure 1.

Yeast two-hybrid system LexABD/ Gal4AD was used to assess protein interaction. The interaction between proteins fused with LexABD and Gal4AD drives reporter gene "HIS3" expression. Yeast cells expressing fusion protein LexABD-Dnm1 and Gal4AD-Srv2 were assayed for growth on SD-His plate (serial dilution as indicated at the top).

.

Supplemental Figure 2.

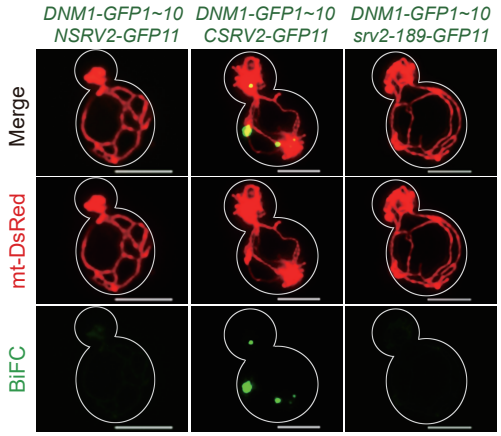

Figure S2. BiFC analysis for assessing interaction between truncated/ mutated Srv2 and Dnm1, related to Figure 1.

Bimolecular fluorescence complementation (BiFC) experiments were used to analyze interaction between N/C-terminal Srv2 and *srv2-189* and Dnm1. Yeast transformed with DNM1-GFP1~10+ NSRV2-GFP11, DNM1-GFP1~10+ CSRV2-GFP11, or DNM1-GFP1~10+ *srv2-189*-GFP11 were examined using BiFC assays. To improve the poor BiFC signals, NSRV2-GFP11/ CSRV2-GFP11/ *srv2-189*-GFP11 were expressed by pRS425 vector (2-micron plasmid). mt-DsRed was expressed to label mitochondria. Scale bars denote 5 μm.

Supplemental Figure 3.

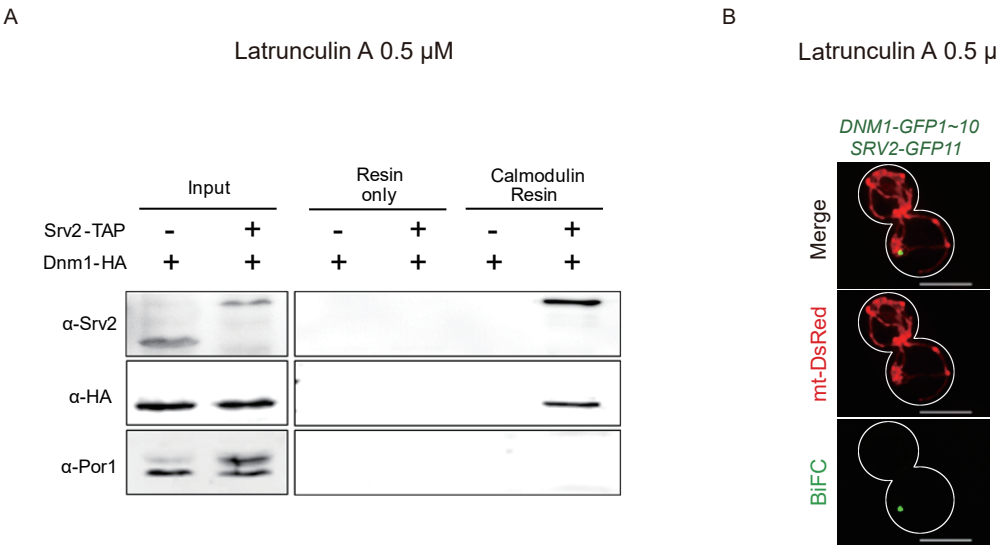

Figure S3. Latrunculin A treatment does not disrupt Srv2-Dnm1 interaction, related to Figure 5.

Co-Immunoprecipitation (Co-IP) and bimolecular fluorescence complementation (BiFC) combined with latrunculin A (Lat-A) were used to assess Srv2 Dnm1 interaction upon disrupted actin dynamics. (A) The same strains and materials as in Figure 1B combined with 0.5 μM Lat-A were used to perform Co-IP experiments. (B) Yeast transformed with SRV2-GFP11 and DNM1-GFP1~10 combined 0.5 μM Lat-A were used to perform BiFC experiments. The results indicated that 0.5 μM Lat-A does not disrupt Srv2-Dnm1 interaction.

Supplemental Figure 4.

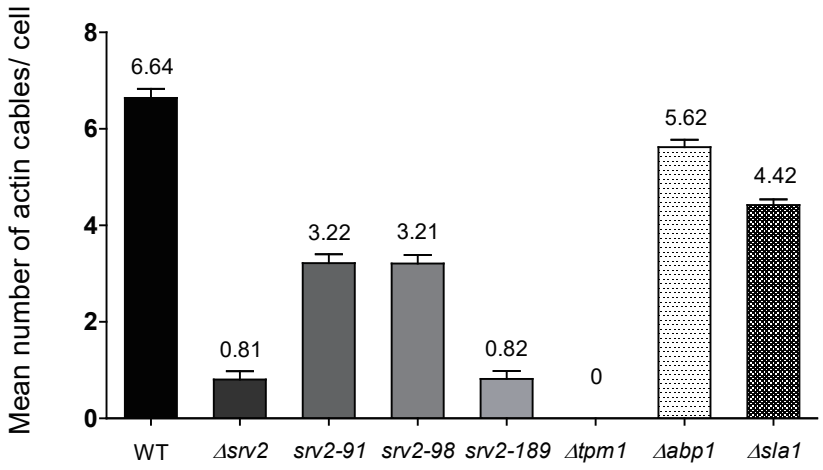

Figure S4. Actin cable counts in different yeast strains, related to Figure 5.

WT, *srv2* mutants, actin cable mutant (*Δtpm1*) and actin patch mutants (*Δabp1* and *Δsla1*) were grown at 30 °C in YPD, fixed and stained with rhodamine phalloidin. Visible actin cables in mother cell were counted (n≧50 cells per strain).

Supplemental Figure 5.

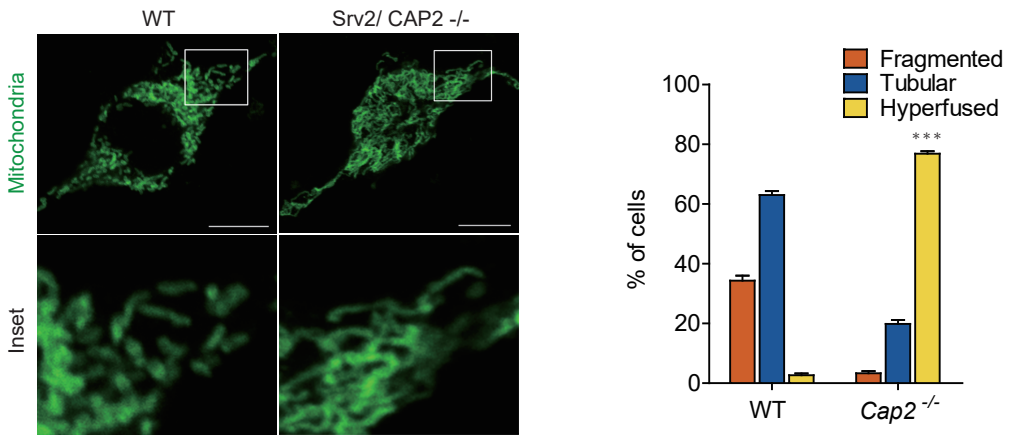

Figure S5. Mitochondrial elongation and hyperfusion in CAP2-/- Human neuroblastoma SH-SY5Y cell line, related to Figure 2.

The CAP2$^{-/-}$ SH-SY5Y cell line was generated by CRISPR/ Cas9 system. Mitochondrial network morphology in wild-type (WT) and CAP2$^{-/-}$ cells expressing mito-EYFP was examined by fluorescence microscopy. The ratios of WT and CAP2$^{-/-}$ cells with hyperfused mitochondria were: WT, 2.67 % and CAP2$^{-/-}$, 76.83 %. Statistical data for each strain were obtained from three trials of 100 cells. The mean values ± SE were obtained by averaging the percentages of three counts. ***$p<0.001$ vs. WT group. Scale bars denote 10 μm.

Supplemental Figure 6.

A

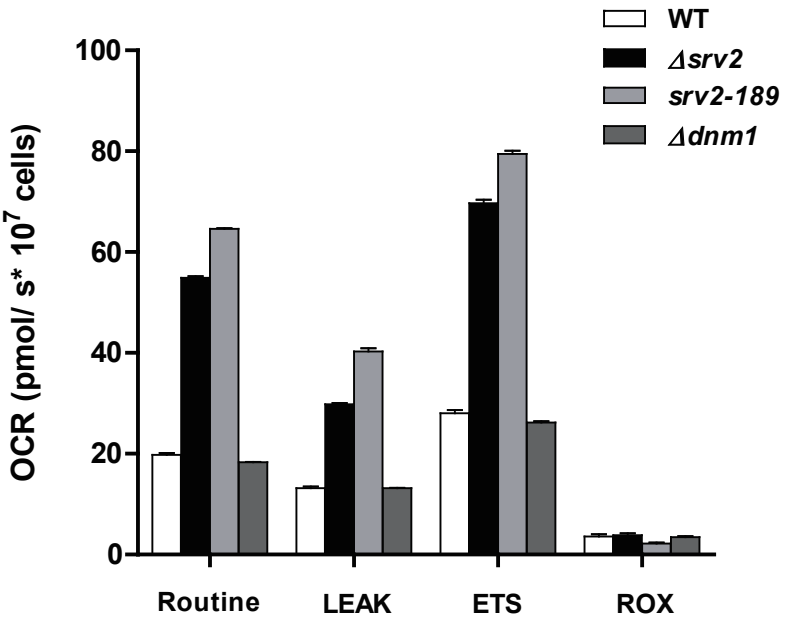

Figure S6 Oxygen consumption rates (OCR) are different among yeast strains, related to Figure 6.

OCR in different yeast strains under basal conditions or the addition of TET (ATP synthetase inhibitor), FCCP (uncoupler, proton carrier), and Antimycin A (complex III inhibitor) were measured by high resolution respirometry. Routine denotes OCR in the basal condition. LEAK denotes OCR with TET treatment, which reflects futile oxygen consumption even though ATP synthesis is blocked. ETS denotes OCR after FCCP titration, which causes proton loss and drive mitochondria consume more oxygen to replenish the proton gradient. ROX denotes OCR in Antimycin A treatment, which depletes OCR derived from mitochondria respiration and reveals oxygen consumption in this system other than mitochondria.

Supplemental Table 1. Yeast strains and their genotypes used in this study, related to Figure 1, 2, 3, 4, 5 and 6.

Strain	Genotype
WT	W303-1A
Δ*srv2*	W303-1A, Δ*srv2:: KanMX*
HIS3::SRV2	W303-1A Δ*srv2:: KanMX pSRV2::HIS3*
Gal::SRV2	W303-1A, Δ*srv2:: KanMX GalSpSRV2::HIS3*
Δ*dnm1*	W303-1A, Δ*dnm1::HPH*
Δ*fzo1*	W303-1A, Δ*fzo1:: HPH*
Δ*srv2*Δ*dnm1*	W303-1A, Δ*srv2:: KanMX* Δ*dnm1::HPH*
Δ*srv2*Δ*fzo1*	W303-1A, Δ*srv2:: KanMX* Δ*fzo1::HPH*
srv2-91	W303-1A, Δ*srv2:: KanMX psrv2-91::HIS3*
srv2-98	W303-1A, Δ*srv2:: KanMX psrv2-98::HIS3*
srv2-189	W303-1A, Δ*srv2:: KanMX psrv2-189::HIS3*
DNM1-HA	JSY1542
SRV2-TAP, DNM1-HA	JSY1542, *SRV2-TAP::HIS3MX6*
Δ*srv2, DNM1-HA*	JSY1542, Δ*srv2:: KanMX*
DNM1-GFP	W303-1A, *DNM1-GFP::HIS3MX*
Δ*srv2, DNM1-GFP*	W303-1A, Δ*srv2:: KAN DNM1-GFP::HIS3MX*
Δ*fis1, DNM1-GFP*	W303-1A, Δ*fis1:: HPH DNM1-GFP::HIS3MX*
Δ*tpm1*	W303-1A, Δ*tpm1::KanMX*
Δ*abp1*	W303-1A, Δ*abp1::KanMX*
Δ*sla1*	W303-1A, Δ*sla1::KanMX*

Supplemental Table 2. Plasmids used in this study, related to Figure 1, 2, 3, 4 and 5.

Plasmid ID	Description
pVT100U-mtGFP	Matrix-targeted GFP expression
pVT100U-mtDsRed	Matrix-targeted DsRed expression
pRS403-pSRV2	For *SRV2* gene integration
pRS403-GalSSRV2	For *GalSpSRV2* integration
pRS403-psrv2-91	For *srv2-91* allele integration
pRS403-psrv2-98	For *srv2-98* allele integration
pRS403-psrv2-189	For *srv2-189* allele integration
pRS425-ADH-NSRV2	For N-terminal Srv2 overexpression
pRS425-ADH-CSRV2	For C-terminal Srv2 overexpression
pRS425-ADH-PFY1	For Pfy1 overexpression
pRS413-pSRV2-GFP11	For Bimolecular fluorescence complementation
pRS414-pDNM1-GFP1-10	For Bimolecular fluorescence complementation
pRS414-pFZO1-GFP1-10	For Bimolecular fluorescence complementation
pRS425-pNSRV2-GFP11	For Bimolecular fluorescence complementation
pRS425-pCSRV2-GFP11	For Bimolecular fluorescence complementation
pRS425-psrv2-189-GFP11	For Bimolecular fluorescence complementation

Transparent Methods

Yeast Strains and Genotypes

All yeast strains and genotypes used in this study are listed in Supplemental Table 1. Gene deletion strains and *DNM1-GFP* tag-related strains were constructed based on *S. cerevisiae* W303-1A (RRID: SCR_003093). Gene deletion strains were constructed mainly by PCR-based gene replacement with a *KanMX4* cassette that was amplified from the yeast deletion collection. For double-gene deletion strains, the *KanMX4* cassette was replaced by *HIS3MX6* or *HphMX4* cassettes from a yeast GFP collection or pAG32. The *KanMX4* cassette was then used again to construct the second gene deletion. For *DNM1-GFP* fusion strains, *GFP* with a *HIS3MX6* cassette was integrated proximal to the stop codon of *DNM1* by PCR-mediated homologous recombination. For construction of strains CYC005, CYC016, CYC018, and CYC046, the integrative plasmids pRS403-*pSRV2*, pRS403-*psrv2-91*, pRS403-*psrv2-98*, and pRS403-*GalSpSRV2* were linearized by restriction digestion for integration at the *HIS3* locus after yeast transformation.

Plasmid Constructions

All plasmids used in this study are listed in Supplemental Table 2. pRS425-ADH1 was constructed by amplifying the *ADH1* promoter from pGAD424 and cloning into

pRS425. Subsequently, DNA fragments encoding *N-SRV2* (residues 1-259), *C-SRV2* (residues 253-526), and *PFY1* were amplified from yeast genomic DNA and then cloned into pRS425-ADH1 to generate pRS425-ADH1-*N-SRV2,* pRS425-ADH1-*C-SRV2*, and pRS425-ADH1-*PFY1*. pRS403-*pSRV2* was constructed by amplifying the open reading frame (ORF) of the *SRV2* gene along with the upstream 490 base pairs from yeast genomic DNA and cloning into the pRS403 vector. Based on previous studies (Chaudhry et al., 2010, Chaudhry et al., 2013), pRS403-*psrv2-91* and pRS403-*psrv2-98* were generated by PCR-mediated mutagenesis from pRS403-*pSRV2* using primers (*srv2-91*: CACAGTTTTGGACTAATGCTATTGCTGCTGCTTACAGAGAGTCTGATC and GATCAGACTCTCTGTAAGCAGCAGCAATAGCATTAGTCCAAAACTGTG/ *srv2-98*: GAAAATATCACTAAGGGTGCTGCTGCTGCTGACAAATCCCAACAAAC and GTTTGTTGGGATTTGTCAGCAGCAGCAGCACCCTTAGTGATATTTTC). pRS403-*psrv2-189* was generated by PCR-mediated mutagenesis with both sets of primers. For construction of pRS403-*GalSpSRV2*, the DNA fragment containing the *GalS* promoter and *SRV2* ORF was amplified from pRS414-*GalSpSRV2*. For pVT100U-mtDsRed construction, the GFP in pVT100U-mtGFP was replaced by a DsRed sequence amplified from DCY2370 (the yeast strain containing *DNM1-GFP*

and mtDsRed, a gift of Dr. David Chan, California Institute of Technology). For plasmids used in the bimolecular fluorescence complementation (BiFC) assay, DNA fragments of split-GFP (GFP1-10/ GFP11) were amplified from pcDNA3.1-MFN2-sfGFP11 and pcDNA3.1-sfGFP1~10 (gifts from Dr. Tzu Kang Sang, National Tsing Hua University). DNA fragments encoding individual proteins and native promoters were ligated to either GFP1-10 or GFP11 DNA fragments. Ligated DNA fragments were cloned into pRS413 and pRS414 (low-copy vectors), as shown in Supplemental Table 2.

Microscopy

Yeasts were examined during the log phase of growth in medium containing either glucose or galactose. Fluorescence images were captured using an inverted microscope (Zeiss/Observer.Z1) with a 63× objective lens (Zeiss Plan-ApoChromat 63×) and AxioVs40 software. Mitochondria were visualized by expressing matrix-targeted Su9-EGFP from pVT100-mtGFP (Westermann and Neupert, 2000) or matrix-targeted Su9-DsRed from pVT100-mtDsRed. For colocalization analysis of Dnm1 and mitochondria, *z*-section images captured by fluorescence microscopy were projected (orthogonal projection, maximum) using ZEN 2012 image acquisition software. Each individual yeast cell in the projected image was analyzed separately

with ImageJ software (NIH) and the plugin “Manders Coefficients”. For actin cable and patch staining, yeasts were fixed in medium containing 3.7% formaldehyde for 15 min at room temperature, washed with phosphate buffered saline (PBS), and stained in PBS containing 0.165 μM rhodamine phalloidin. Actin cable counts were based on the previous published paper (Alioto et al., 2016, Higuchi-Sanabria et al., 2016). For latrunculin A treatment, yeast cells were incubated with medium containing 0.5 μM latrunculin A for 6 h. For galactose induction, CYC005 was inoculated in SC medium containing 2% raffinose until the log phase of growth. The yeast cells were then transferred to YP medium containing 2% galactose for 3 h.

Tandem affinity purification (TAP) tag co-precipitation

Yeasts with TAP tag grown to mid-log phase were harvested by centrifugation. Pellets were washed with ddH_2O and resuspended with extraction buffer (10 mM Tris-Cl, pH 8.0, 1 mM dithiothreitol (DTT), 150 mM NaCl, 1 mM magnesium acetate, 1 mM imidazole, 2 mM $CaCl_2$, 0.1% NP-40). Glass beads were added to break the yeast cells during vortexing for 15 min at 4 °C. Supernatants were collected thoroughly from cell lysates by centrifugation at 15,000 *g*. Aliquots (150 μL) of the resulting supernatant were incubated with 25 μL of bovine serum albumin pre-coated calmodulin Sepharose beads for 3 hr at 4 °C. After incubation, the Sepharose beads were washed

three times with wash buffer (10 mM Tris-Cl, pH 8.0, 1 mM DTT, 500 mM NaCl, 1 mM magnesium acetate, 1 mM imidazole, 2 mM $CaCl_2$, 0.1% NP-40). The Sepharose beads were incubated with elution buffer (10 mM Tris-Cl, pH 8.0, 1 mM DTT, 150 mM NaCl, 1 mM magnesium acetate, 1 mM imidazole, 2 mM EGTA, 0.1% NP-40) for 5 min. The Sepharose beads with elution buffer and protein sample buffer were boiled for 5 min and cooled. The supernatants were collected for further western blot analysis.

BiFC Assay

To detect specific interaction between Srv2 and Dnm1 in yeasts, plasmids pRS413-pSRV2-GFP11 and pRS414-pDNM1-GFP1-10 were transformed in the specific strains described; the plasmids were constructed with low-copy vectors (yeast centromere plasmids) and native promoter. To avoid the titration effects of endogenous protein (without the split-GFP moiety), the indicated gene deletion strains were used in these experiments. For example, the Δsrv2 Δdnm1 yeast strain transformed with pRS413-pSRV2-GFP11 and pRS414-pDNM1-GFP1-10 was used to detect the interaction of Srv2 and Dnm1. pVT100-mtDsRed was also used for labeling mitochondria.

Mitochondrial Fractionation

Mitochondria crude extracts were obtained by yeast cell fractionation (Meisinger et al., 2006). Briefly, yeast cells grown to mid-log phase were harvested by centrifugation at 1,500 g and suspended in DTT buffer at 30 °C for 20 min. The cells were washed and resuspended in buffer containing zymolyase for 30 min. Zymolyase-treated yeasts (spheroplasts) were collected by centrifugation, resuspended in homogenization buffer, and homogenized with 15 strokes of a glass-Teflon homogenizer. The homogenates were centrifuged at 1,500 g to pellet cell debris and nuclei, and the supernatants were collected and centrifuged at 4,000 g and then at 12,000 g. The pellets were denoted as the "crude mitochondria fraction", and supernatants were denoted as the "cytosolic fraction". Protein in both fractions were then analyzed by western blotting.

Flow Cytometry

Mitochondrial membrane potential was evaluated by DiOC6(3) staining (Cat. D273, Life Technology). Yeasts were incubated in medium containing 175 nM DiOC6 (3) for 20 min at 30 °C in the dark. Samples were evaluated using an Accuri C6 flow cytometer (BD Bioscience) following the protocol provided by the company. Data were analyzed using Cellquest software from BD Bioscience.

High-resolution Respirometry

Yeasts oxygen consumption rates were determined using an Oxygraph-2K (Oroboros). Data was analyzed by DatLab software provided by the company. Yeasts grown to stationary phase in Yeast Extract Peptone Dextrose Medium (YPD) were subcultured (160× dilution) in YPD/YPR (raffinose as carbon source) until an optical density at 600 nm of 0.6. The inoculates were then mixed with YPD/ YPR at a concentration of 5 × 10^6 cells per mL. The examination was done using 10^7 cells. Triethyltin bromide (TET, 150 μM), carbonilcyanide p-triflouromethoxyphenylhydrazone (FCCP, < 4 μM), and 2 μM antimycin A were added stepwise. Mitochondrial basal respiration (R), proton leakage (L), and maximal respiration (E) can be evaluated by determining oxygen consumption rates with these mitochondrial inhibitors. To compare the mitochondrial functionality of yeast strains with different basal respiration (routine oxygen consumption), the oxygen consumption rates were transferred to comparable values, designated as the reserve capacity, by calculating (E-R)/E.

Phylogenetic Analysis

Protein sequences of the indicated species were obtained from the Uniprot website (http://www.uniprot.org/). These sequences were aligned, curated, and

phylogenetically analyzed using the MUSCLE online software, Gblocks, and PhyML, respectively (Edgar, 2004, Castresana, 2000, Dereeper et al., 2010, Guindon and Gascuel, 2003). The phylogenetic tree was generated using TreeDyn (Chevenet et al., 2006). Software was accessed at http://www.phylogeny.fr/.

Statistical Analysis

All experiments were conducted with at least three independent trials. To classify mitochondrial morphology, more than 100 cells were examined in each trial. Data are expressed as mean values. All error bars in the figures represented standard error unless otherwise specified. Significance was determined using two-tailed, unpaired Student's *t* tests.

Supplemental References

ALIOTO, S. L., GARABEDIAN, M. V., BELLAVANCE, D. R. & GOODE, B. L. 2016. Tropomyosin and Profilin Cooperate to Promote Formin-Mediated Actin Nucleation and Drive Yeast Actin Cable Assembly. *Curr Biol,* 26**,** 3230-3237.

CASTRESANA, J. 2000. Selection of conserved blocks from multiple alignments for their use in phylogenetic analysis. *Mol Biol Evol,* 17**,** 540-52.

CHAUDHRY, F., BREITSPRECHER, D., LITTLE, K., SHAROV, G., SOKOLOVA, O. & GOODE, B. L. 2013. Srv2/cyclase-associated protein forms hexameric shurikens that directly catalyze actin filament severing by cofilin. *Mol Biol Cell,* 24**,** 31-41.

CHAUDHRY, F., LITTLE, K., TALARICO, L., QUINTERO-MONZON, O. & GOODE, B. L. 2010. A central role for the WH2 domain of Srv2/CAP in recharging actin monomers to drive actin turnover in vitro and in vivo. *Cytoskeleton (Hoboken),* 67**,** 120-33.

CHEVENET, F., BRUN, C., BANULS, A. L., JACQ, B. & CHRISTEN, R. 2006. TreeDyn: towards dynamic graphics and annotations for analyses of trees. *BMC Bioinformatics,* 7**,** 439.

DEREEPER, A., AUDIC, S., CLAVERIE, J. M. & BLANC, G. 2010. BLAST-EXPLORER helps you building datasets for phylogenetic analysis. *BMC Evol Biol,* 10**,** 8.

EDGAR, R. C. 2004. MUSCLE: multiple sequence alignment with high accuracy and high throughput. *Nucleic Acids Res,* 32**,** 1792-7.

GUINDON, S. & GASCUEL, O. 2003. A simple, fast, and accurate algorithm to estimate large phylogenies by maximum likelihood. *Syst Biol,* 52**,** 696-704.

HIGUCHI-SANABRIA, R., VEVEA, J. D., CHARALEL, J. K., SAPAR, M. L. & PON, L. A. 2016. The transcriptional repressor Sum1p counteracts Sir2p in regulation of the actin cytoskeleton, mitochondrial quality control and replicative lifespan in Saccharomyces cerevisiae. *Microb Cell,* 3**,** 79-88.